Review

# Recent Advances of AIEgens for Targeted Imaging of Subcellular Organelles

SONG Nan[1,2], XIAO Peihong[1,2], MA Ke[1,2], KANG Miaomiao[1,2], ZHU Wei[1,2], HUANG Jiachang[1,2], WANG Dong[1]✉ and TANG Ben Zhong[3]✉

Received December 19, 2020
Accepted January 4, 2021


Fluorescence imaging based on luminogens with aggregation-induced emission(AIE) effect has drawn great attention in recent two decades, due to their superior advantages to overcome the technical difficulties. Thus, the AIE-active bioprobes with targeted ability at the subcellular level have been widely investigated to visualize the subcellular structures and monitor the biological processes. Considering the very rapid developments and the significance of selective imaging of subcellular structures, we summarize the recent two-year achievements about the AIEgens for targeted imaging of subcellular organelles including nuclei, membranes, lipid droplets(LDs), endoplasmic reticulum(ER), lysosomes, mitochondria and cytoplasm. The designed protocols and advantages of AIEgens, their mechanisms for targeted staining at organelles and the imaging performance are discussed. These AIE bioprobes exhibit great potentials for early diagnosis and therapeutics of diseases that related to subcellular organelles. Finally, the perspectives about AIEgens for these applications are also discussed.

**Keywords** Aggregation-induced emission; Monitoring bioprocess; Subcellular organelles; Targeted ability; Theranostics

## 1 Introduction

As the essential building blocks, trillions of cells constitute the living organisms and human bodies to guarantee the organic functionalities and basic life-support. Various biochemical processes occur within diverse cells every moment. Thus, it is of significance to maintain the normal metabolism and functionalities of cells[1]. Animal cells are sophisticated and subtle systems, mainly consisting of cytoplasm, nucleus and cell membranes to surround cells as boundaries. There are cytoplasm matrix and subcellular organelles in cytoplasm, including lysosomes, mitochondria, endoplasmic reticulum (ER), lipid droplets(LDs) and Golgi apparatus[2]. The multiple components, organelles and signal molecules work together to adjust the cellular metabolism and genetics, so that the life activities can be self-regulated and proceed in high-order performance to adapt to various environment. Every organelle performs its own functions[3,4]. For instance, nucleus is a small sphere in cytoplasm with nucleopore, which is the location of genetic information; LDs are the main storage sites for neutral lipids, which are widely found in bacteria, yeast, insects and animal cells; ER always works as a workshop for protein processing and lipid synthesis; lysosome is the workshop for digestion, which possesses abundant hydrolytic enzymes and acidic microenvironment; mitochondria is the power shop for aerobic respiration of cells, in which 95% of the energy is generated to maintain the cellular activities; Golgi apparatus plays a vital role in the transportation of secreted proteins, where the synthesized proteins are reprocessed, classified and packaged[5−8]. Consequently, the blueprints of morphologies and functions of these structures are significant for a detailed understanding of the specific process and the pathways in biosystems, as well as taking a deep insight into the pathogenesis of miscellaneous diseases, which will facilitate to develop the novel theranostics especially for the incurable diseases[9−12]. However, the techniques are still limited to study their structures due to their size and complicated environment within cells, even though we have already known them for a long time[13].

Fluorescence imaging, as a super-fast and non-invasive technique, plays an important role in bioimaging, which makes it possible for visualization of subcellular structures and monitoring the biological processes in the real-time model[14,15]. The development of fluorescent bioprobes for specific visualization of subcellular organelles enables the study and monitoring of the locations, morphologies and changes that reveal the biological dysfunction. However, the conventional fluorescence bioprobes undergo the aggregation-caused quenching(ACQ) phenomenon, resulting in the self-quenching of emission when the hydrophobic ACQ dyes enter into the intracellular environment due to the aggregation[16]. Thus, weak fluorescent signals with a low signal to noise ratio can be detected, especially in the tiny subcellular organelles[17].

✉ WANG Dong
wangd@szu.edu.cn
✉ TANG Ben Zhong
tangbenz@ust.hk
1. Center for AIE Research, Shenzhen Key Laboratory of Polymer Science and Technology, Guangdong Research Center for Interfacial Engineering of Functional Materials, College of Material Science and Engineering, Shenzhen University, Shenzhen 518060, P. R. China;
2. College of Physics and Optoelectronic Engineering, Shenzhen University, Shenzhen 518060, P. R. China;
3. Department of Chemistry, The Hong Kong University of Science and Technology, Clear Water Bay, Kowloon, Hong Kong, P. R. China

Fortunately, a class of luminogens with optical properties different from ACQ dyes have been identified and reported by Tang and coauthors in 2001[18−23], named as aggregation-induced emission(AIE) luminogens(AIEgens). In contrast to ACQ luminogens, AIEgens exhibited negligible fluorescence emission when dispersing and enhanced-emission in aggregated/solid state, caused by the restriction of intramolecular motions(RIMs) that blocking the radiative decay and facilitating the non-radiative decay[24−27]. During the past 20 years, large amounts of AIEgens, with a whole-range of wavelengths, tunable brightness and excellent biocompatibility, have been designed and synthesized to satisfy multitudinous demands in many fields, especially in biological science[28−33]. Well-designed bioprobes with AIE effect have come to our sight for multiple imaging in cells. AIEgens exhibit outstanding performance in monitoring the intracellular structures, incorporating with therapeutic outcomes frequently[34,35]. Thus, in this review, we summarized the latest advances about AIEgens for targeted imaging of subcellular organelles within two years. The advantages of AIEgens to visualize the important organelles and the simultaneous therapeutics will be fully discussed(Fig.1). Besides, the main research bottleneck of AIEgens with target ability and future perspectives will also be discussed briefly.

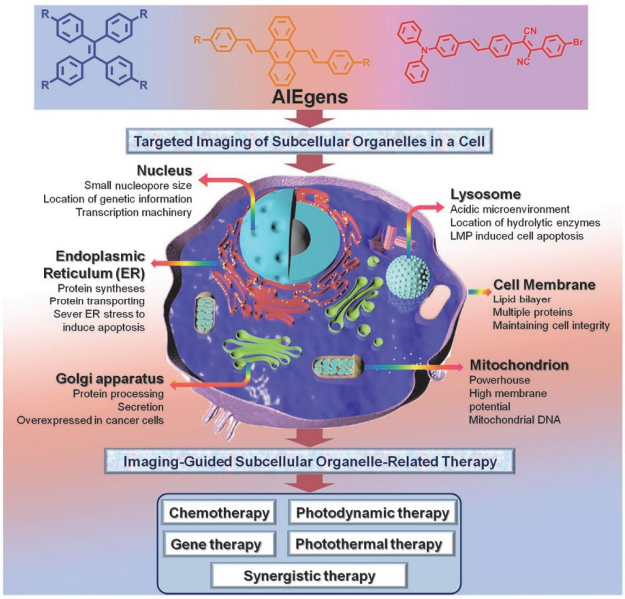


**Fig.1 Schematic illustration of AIE-active bioprobes that can be used for targeted imaging of subcellular organelles**

Top: chemical structures of representative AIEgens; middle: the anatomy of a mammalian cell; bottom: AIEgens for imaging-guided subcellular organelle-related theranostics.

## 2 Nucleus

The nucleic acids, such as DNA and RNA, mainly locate in the cell nucleus and play a significant role in genetic technology. The commercial nucleic acid dyes(such as Hoechst and DAPI) are mainly intercalators, which are water-soluble and have a high affinity for the cell nucleus[36,37]. But their cytotoxicity is high and not suitable for long-term imaging. In contrast, many water-soluble AIE-active probes with rather low cytotoxicity have been designed for cell nucleus imaging by using different interaction mechanism, containing electrostatic interaction, intercalation, and specific connection site[38].

Most AIE-active probes have electrostatic interaction with nucleic acids. Tang *et al*.[39] reported two positively charged tetraphenylethene derivatives(blue emission) with trimethylammonium groups or triethylammonium groups for nucleus imaging of dead cells. But they could not penetrate the cell membrane and stain the live cell nucleus. Zhou's group[40] reported a similar work, in which a *p*-phenylenediacetonitrile derivative(green emission) with the positive charge for dead cell nucleus imaging was demonstrated. To improve the membrane penetration ability of the AIE-active probes, Ma and coworkers[41] elaborately designed triphenylamine derivatives (red emission) with different amounts of pyridiniums and boric acid groups for live cell nucleus imaging. It was found that the probe with three positively-charged pyridiniums and boric acid groups possessed wonderful membrane permeability and specifically enriched into the nucleus. And the long lifetime(4.9 ns) made this probe befitting for the cellular visualization in time-resolved imaging.

To further investigate the apoptosis monitoring process, a set of positively charged tetraphenylethene derivatives(red emission) as highly active photosensitizers with the photodynamic therapy(PDT) ability was developed[Fig.2(A)][42]. It can be observed that only the AIE-active probe with four pyridiniums(TPE-4EP+) could transfer from mitochondria to the nucleus under the apoptosis process, owing to its highest PDT effect[Fig.2(B)]. The mechanism of this probe translocation was induced by photodynamic therapy(PDT). Firstly, this positively charged probe stained the negatively charged mitochondrial membrane *via* electrostatic interaction. Then PDT effect induced the cell apoptosis, thus the mitochondrial membrane potential depolarization occurred, and the membrane permeability increased. Finally, this positively charged probe lost the targeting ability after mitochondrial dysfunction, then rapidly penetrated into the cell nucleus through strong electrostatic interaction. As shown in Fig.2(C)—(F), fixed HeLa cells can be stained with TPE-4EP+, DAPI(nucleus dye) and MTO(mitochondria dye). These fixed cells underwent an apoptosis process, thus TPE-4EP+ probes were located on the cell nucleus, not mitochondria. In comparison, the other two probes showed no translocation ability and apoptosis monitoring because they had weak electrostatic interaction with DNA[Fig.2(G)]. Only the molecules with more pyridinium moieties could bond to the negatively charged DNA by electrostatic interaction. This work can assist to control the phototoxicity dose and minimize the


https://doi.org/10.1007/s40242-021-0430-1

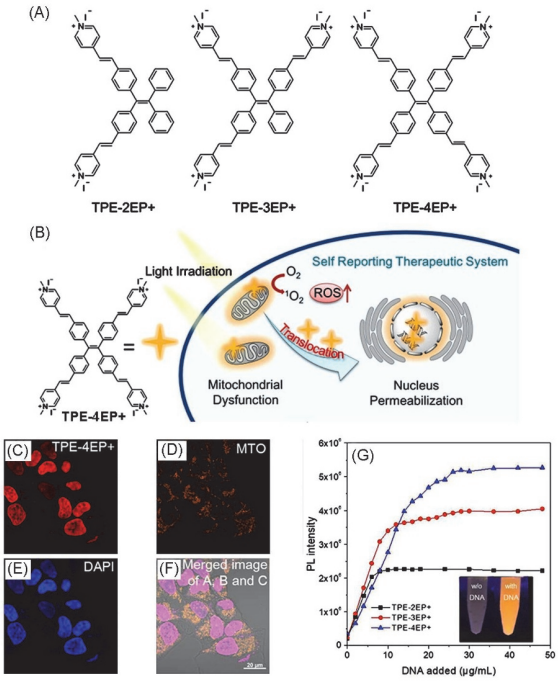


**Fig.2 Chemical structures of three positively charged TEP derivatives(A), mechanism of the nucleus-targeting imaging(B), imaging of HeLa cells incubated with TPE-4EP+(C), MTO(D) and DAPI(E), merged images of (C), (D) and (E)(F) and changes of fluorescence intensity at a wavelength of 605 nm upon adding ctDNA(G)**

Inset of (G): photographs of TPE-4EP+ with and without the ctDNA.
Reprinted with permission from Ref.[42], Copyright 2019, American Chemical Society.

potential side effect[42]. In addition, a controllable supramolecular assembly within living cells was reported. Two peptides modified molecules underwent a programmed process, resulting in the fibrillar structure assembly in the live cells. These fibrillar assemble complexes presented blue emission and could interact with nucleolus through electrostatic and hydrophobic interactions. Therefore, it is an innovative way to explore how the synthetic assembly can impact a living system[43].

Several reported AIE-active probes can interact with nucleic acids by intercalation or specific connection site. Tang and coworkers[44] reported a bicolourable AIEgen for nucleolus staining and mitochondria staining. An $\alpha$-cyanostilbene derivative can visualize mitochondria with yellow or orange color through the electrostatic interaction between the probe pyridinium unit and mitochondria. While this probe also had intercalation with the nucleus, and the emission presented a red-shift in the nucleolus as well. However, the emission ranges of the two organelles had a large overlap, which was difficult to eliminate. Liu and coworkers[45] developed a TPE derivative for live cell nucleus imaging through the specific connection site. This blue emission probe was functionalized with a special peptide, which had the cell penetration property and the nucleus localization site. This low cytotoxicity probe was desirable for long-term nucleus imaging, but the high cost of the purification and synthesis limited its applications. Chen *et al*.[46] designed a novel AIEgen named ID-IQ for cytogenetic study. This yellow emission probe had the special connection site with chromosome periphery, thus could sharply highlight the chromosome boundaries, not the whole genome. Therefore, it realized the distinct visualization of the chromosome mitosis process, and could act as a versatile cytogenetic tool for *in situ* hybridization genomic research.

However, the chromosome periphery imaging in live cells remains a challenge by using this probe[46]. To improve the cell transfection efficiency for gene delivery, a smart non-viral gene vector with AIE-active two-photon absorption property was designed. As shown in Fig.3, 2,3-dicarboxylate-5,6-diphenylpyrazine(DEDPP) derivatives acted as the AIE core, which had the gemini surfactant structure and the two-photon absorption property[47]. The hydrophilic section triazole-[12]aneN$_3$ and the hydrophobic section long alkyl chains were modified on the AIE core, respectively. In the aqueous solution, these DEDPP derivatives self-assembled into a micelle with different diameter sizes. It acted as a gene vector through the electrostatic interaction between triazole-[12]aneN$_3$ group and DNA. After the self-assembly with DOPE(dioleoylphosphatidyl ethanolamine), a lipoplex was achieved to enhance the cell transfection efficiency. This lipoplex could penetrate into the cell by a micropinocytosis pathway. The lipoplex structure would be broken by the ester bond cleavage of DEDPP derivatives due to lipase, thus resulting in DNA complexes escape. Then DNA complexes entered into the cell nucleus, and the pH change in the nucleus environment might break the pH-responsive ester bonds of triazole-[12]aneN$_3$ groups, leading to DNA release in the nucleus. If delivery DNA was labeled with a red commercial dye, the nucleus could be stained with red color of the

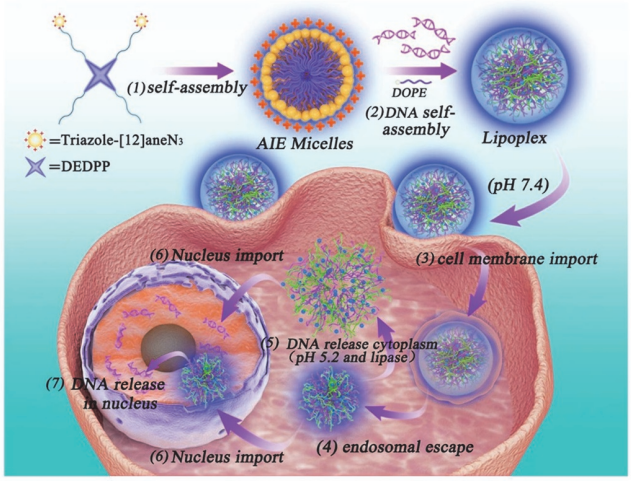


**Fig.3 Representation of the nucleus-targeted imaging and gene delivery of lipoplex**

Reprinted with permission from Ref.[47], Copyright 2020, American Chemical Society.

commercial dye and blue color of DEDPP molecules after 3 h. Moreover, the DEDPP molecules were excreted in the metabolic process after 6 h staining, and red color of the labeled DNA remained. This vector provides a high cell transfection efficiency to deliver DNA into the cell nucleus with low cytotoxicity. However, the vector structure is still too complicated, and needs to be simplified(Fig.3).

## 3 Cell Membranes

The cell membrane(also called the plasma membrane or cytoplasmic membrane), as a barrier to protect intracellular environments, protects the integrity of the cell and plays a key role in the biological system[48]. The cell membrane is mainly comprised of amphiphilic phospholipids bilayers, displaying a large negative potential across the membrane. Therefore, dyes targeted in the cell membranes are usually amphiphilic or cationic[49], such as the commercial cell membrane dyes DiO and DiI. Tong and Shuai *et al.*[50] prepared an amphiphilic and cationic AIE probe, *i.e.*, TPNPDA-C12, with TICT effect and a suitable critical micelle concentration(Fig.4)[50]. The TPNPDA-C12 probe has dual-colored fluorescence, which could simultaneously and selectively stain two different organelles through distinct fluorescence channels. TPNPDAC12 fused into the cell membrane by amphiphilic interaction, and the restricted monomers exhibited red fluorescence. On the other hand, TPNPDA-C12 could stain mitochondria to show yellow fluorescence through electrostatic interaction. The alkyl chain length of TPNPDA analogues is critical for their distribution in the subcellular organelles due to the influence of the hydrophobicity and hydrophilicity of the molecules. Additionally, TPNPDA-C12 could dynamically visualize cell membranes *via* ROS- and cytotoxin-induced cell apoptosis and necrosis. Besides, Tian *et al.*[51]. fabricated two-photon absorption fluorophores with the same positively charged 1-(2-hydroxyethyl) pyridinium core and various electron-donating terminal groups. The fluorophore featuring *N*,*N*-dibutylbenzenamine(2HP-BA) as an electron-donating group possessed good membrane permeability with obvious AIE characteristics, and exhibits effective two-photon excited fluorescence imaging in living cells.

Changes in cancer cell behavior are generally caused by overexpressed and certain receptors on cell-surface, known as tumor cell-surface markers. Considerable efforts have been made to develop targeting marker technique(*e.g.*, antibodies[52], overexpression of protein-reporter fusions[53], aptamers[54]) for cancer cell membrane imaging. AIEgens modified with corresponding ligands will be beneficial to target cancer cells[55]. For instance, the cyclic arginine-glycine-aspartic acid(cRGD) is a specificity peptide that can target the integrin $\alpha_v\beta_3$ receptors overexpressed in the neovasculature. Liu and Tang *et al.*[56] constructed the first case of cRGD labeled to AIEgen(TPS-2cRGD) for specific integrin $\alpha_v\beta_3$ sensing and cell membrane imaging. More recently, bio-orthogonal click reaction was utilized to decorate cRGD onto the brain tumor cell membrane as a "tactical shell"[57], which can offer blood brain barrier(BBB) penetrating and homotypic targeting effect in the brain tumor microenvironment. The nanocomposite core is composed of conjugated polymer(PDPP3T) and iron oxide nanoparticles,

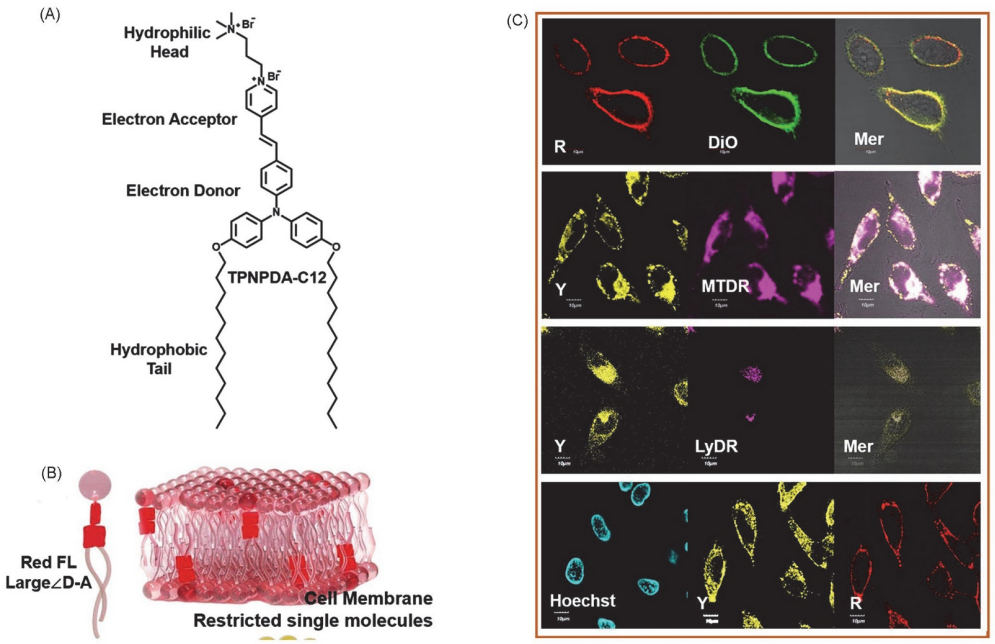


**Fig.4 Structures of TPNPDA-C12(A), schematic illustration of TPNPDA-C12 for the targeted-imaging cell membranes(B) and confocal images of HeLa cells for co-localization of TPNPDA-C12 with DiO(membrane dye), MIDR(mitochondria dye), LyDR(lysosome dye) and Hoechst(nucleus dye)(scale bar is 10 μm)(C)**




https://doi.org/10.1007/s40242-021-0430-1

enabling MRI-FLI-PA multimodal imaging. *In vitro* and *in vivo* results demonstrated the cRGD-labeled brain tumor cell membrane coating possessed admirable targeting outcomes. In addition to targeting cell membranes, AIEgen has the effect of penetrating and eradicating biofilms caused by bacterial infections[58].

## 4 Lipid Droplets(LDs) and Endoplasmic Reticulum(ER)

Lipid droplets(LDs), surrounded by a layer of phospholipid with rich lipids, are mainly distributed in hepatocytes, adrenal cortex and adipocytes. LDs are crucial for various physiological processes, including the formation of neutral lipids, cell activation and apoptosis. Thus, the specific detection and tracking of LDs have attracted abundant interests in the areas of biological medicines and clinical diagnosis.

Recently, various AIE compounds(labeled as A2—A4, B1—B3) with wide color tenability was explored by remoulding an ACQ compound(A1) with rotors[Fig.5(A)][59]. The donor-acceptor(D-A) interaction, enhanced stepwise, was realized by introducing the group of acceptors with an electron-withdrawing feature or changing the donor. In addition, color tunability was also achieved with wide fluorescence emission from blue to red color, covering large regions of visible light. Theoretical calculation further confirmed the increased D-A interaction, consistent with the color tunability. Intriguingly, the hydrophobic compound B3 exhibited specific LDs imaging in PC12 cells and good photostability[Fig.5(B)] because the lipophilic B3 could effectively aggregate in LDs. A strong red fluorescence signal of B3 was observed within cells compared with the controlled cells. Furthermore, co-localization of B3 with BODIPY, as the commercially available LDs bioprobe, was also conducted, indicating excellent targeting ability of B3 toward LDs. Subsequently, B3, with red fluorescence, was further applied for the identification of hyperlipidemia blood, exhibiting great potentials for the diagnosis of cardiovascular diseases. Similarly, the kinetics and dynamics of the organic nanoaggregates, formed from lipophilic 2,1,3-benzothiadiazole(BTD) derivatives, were investigated and decoded[Fig.5(C)], demonstrating that the intramolecular charge-transfer(ICT) and mesomeric forms were important for their AIEE effect. One of the BTD derivatives exhibited selectively imaging for LDs at nanomolar concentration, while the other two also stained LDs at low concentration[Fig.5(D)][60].

Typically, Tang and coauthors[61] explored the mechanism of the required conditions for lipid production *via* visualizing the LDs with a lipid-targeting AIEgen. A novel protocol was developed to detect lipid drops in *E. gracilis* by using the AIE bioprobe, which helped us screen the capacity of lipid droplet production and provided the information about the environmental condition for lipid production. This study paves a new

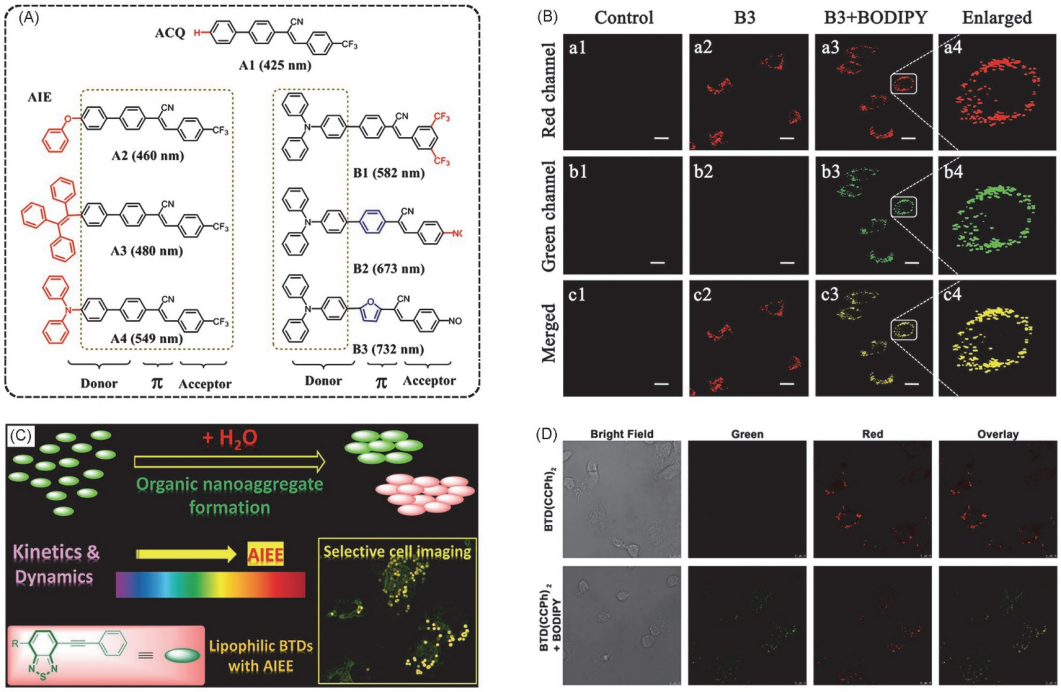


**Fig.5 Chemical structures of A1—A4 and B1—B3(A), confocal images incubated with PBS only(a1—c1), staining with B3(a2—c2), co-localization with B3 and BODIPY Green(a3—c3), enlarged images of co-localization with B3 and BODIPY Green(a4—d4) (B), deciphering the dynamics of nanoaggregating with AIEE effect(C) and confocal images of live cancer cell stained using BTD(CCPh)$_2$, BODIPY and merged images(D)**

(A, B) Reprinted with permission from Ref.[59], Copyright 2020, Royal Society of Chemistry. (C, D) Reprinted with permission from Ref.[60], Copyright 2020, American Chemical Society.


https://doi.org/10.1007/s40242-021-0430-1

way to construct fast-response bioprobes for sources to produce healthy food. In order to satisfy the demands of targeting-guided therapies, natural dihydrobenzo[c]phenanthridine alkaloids of DHCHE and DHSAN were utilized for photoactivatable cancer theranostics due to the photooxidative dehydrogenation reaction upon light irradiation[62]. The hydrophobic DHCHE could selectively accumulate in LDs within cells and then undergo a photoactivatable process to produce CHE with AIE feature, which could monitor the therapeutic process and control the dose of medicine. Inspired by this, more and more promising imaging-guided therapies for diseases related to LDs could be raised.

Endoplasmic reticulum(ER) consists of a large membrane-bound compartment and a single continuous lumen. Recently, the specific labeling of ER has also gained great attraction, because it is an important subcellular organelle for the regulation of calcium ion and protein transport. The dynamic intracellular process related to the balance of protein, intermediates and signaling molecules can be observed *via in situ* ER tracking.

Since the ACQ feature of traditional dyes limited their applications for specific aggregation and imaging in ER, the AIEgens as bioprobes for ER imaging have also been reported. For example, a deep-red AIEgen for tunable organelle-specific staining was designed and synthesized in 2020[63]. The D-A properties of this AIEgen have been strengthened upon modification to change the pyridine to pyridinium, making for the shifting emission to larger wavelengths. In addition, the AIEgen contained a pyridinium-sulfonate group and possessed zwitterionic nature, allowing the applications for organelle targeting. Phosphocholine cytidylyltransferase(CCT) contains multiple positively charged amino acids and is abundant on the membrane of ER, which is a crucial enzyme for the regulation of membrane phospholipid syntheses. The zwitterionic AIEgens were targeted-imaging in various cells including HeLa Cells and 143B cells, while the AIEgens with only positive-charged sites could just stain the mitochondria. This study demonstrates that different organelle-specific imagings could be achieved by designing the molecules with typical platforms regarding such bioimaging probes. Subsequently, an amphiphilic sensor based on quinoline-malononitrile with AIE effect has also been developed for the targeted imaging of ER *via* specific interaction of ATP-sensitive potassium[64]. Attributing to the *p*-toluene sulfonamide group in the AIE-active sensor, the lipophilic dispersity was enhanced and the binding receptor to the ATP-sensitive potassium was successfully anchored.

## 5 Lysosomes

Lysosome is a membrane-bound organelle, which is responsible for the degradation of intracellular and extracellular substances. The composition of lysosome is clear, including membrane and lumen enzymes. There is an acidic environment within lysosome with a pH value of 4.5—5.0, facilitating hydrolysis. Additionally, a lot of cellular processes, such as cholesterol homeostasis, immune response, plasma membrane repair, cell signaling and cell death, involve in lysosomes, making them vital organelles in cells. Lysosomal dysfunction is demonstrated to be related to many diseases. Therefore, the investigation of lysosomes will greatly promote the study of lysosase-related diseases.

Recently, AIE molecules with the ability to target lysosomes have been widely reported. Wu *et al*.[65] have designed and synthesized a D-A-D type molecule(T-BDP) by combinating boron-dipyrromethene and triphenylamine. The emission of T-BDP NPs can cover the near-infrared region in water due to the AIE characteristic. The CLSM images of subcellular localization in cancer cells indicate that T-BDP NPs are mainly localized in lysosomes of cancer cells.

In addition, for fluorescence imaging targeted in lysosomes of tumor cells, multi-modal targeting, such as FLI-PAI-PTI trimodal-imaging of lysosomes, has been further studied and proved to be a powerful tool for imaging-guided theranostics. To achieve this, three novel one-for-all phototheranostics AIEgens(TI, TSI, and TSSI) based on lyso-fluorophores was reported[66]. AIEgens with strong D-A effect and an extended $\pi$-conjugated system were successfully designed and prepared, in which 1,3-bis(dicyanomethylidene)indane was introduced as A group bridged by thiophene with triphenylamine as D group. Furthermore, the introduction of different thiophene rings could regulate the intramolecular distance between D and A, improving the intramolecular rotation and photothermal conversion efficiency in an aggregated state. Aggregated TSSI possessed strong D-A interaction and intramolecular motion, contributing to its excellent abilities for the phototheranostics with NIR-II emission[Fig.6(A)]. Typically, TSSI NPs, as the nanoparticles fabricated from TSSI, had wide absorption including almost the whole NIR-I range, extending a little to 1000 nm. Moreover, the TSSI NPs exhibited NIR-II fluorescence emission within the range of 1000—1200 nm. Benefiting from the outstanding photothermal conversion efficiency, TSSI NPs also exhibited excellent photoacoustic signals according to the *in vivo* experiments. Co-localized imaging indicated that TSSI NPs could specifically staining the lysosomes[Fig.6(B)].

The acidic environment in lysosomes makes it possible for the sensitivity of pH-responsive bonds, which provides great opportunities for the design of drug delivery systems. A novel strategy, based on stimuli-responsive polymeric vesicles, was reported to improve the ROS generation in lysosomes. At acid environment in lysosomes, mPEG-Hyd-PCL-CIN(P-Hyd) loaded with MeTTMN as AIEgens and photosensitizers was cleaved and the disassembly of nano-micelles occurred, resulting


https://doi.org/10.1007/s40242-021-0430-1

in the release of MeTTMN, which was attributed to the pH-responsiveness of mPEG-Hyd-PCL-CIN. Consequently, large amounts of ROS were generated and PDT was also improved[67]. Simultaneously targeting lysosome and mitochondria can significantly enhance the therapeutic effect for the suppression of tumors. To achieve this, Tang and co-workers[68] designed and synthesized anion-$\pi^+$ AIE-active luminogens[Fig.6(C)]. The optical properties indicated that MTBZPy possessed the maximal absorption at the wavelength of 476 nm, which was longer than TBZPy(447 nm). MTNZPy had the longest absorption at 528 nm, due to the strongest intramolecular charge-transfer(ICT). Furthermore, the fluorescent emission signals of TNZPy, MTNZPy, TBZPy, and MTBZPy were detected to be at the wavelength of 662, 686, 625, and 659 nm in THF, respectively. Owing to the introduction of strong ICT structures, two AIE-PSs exhibited high efficiency of ROS generation and excellent outcomes of PDT. Cellular experiments showed that they gradually entered into cells with obvious dynamic processes. The confocal images has shown that these AIE-PSs have great and specific targeting for mitochondria and lysosomes simultaneously[Fig.6(D)]. Intriguingly, because the targeting process was dynamic, AIE-active bioprobes of TNZPy didn't just stay in the same subcellular organelles. The co-staining results revealed that the Pearson's correlation coefficient of TNZPy for lysosomes decreased from 81% to 64%, while the Pearson's correlation coefficients for mitochondria steadily improved from 44% to 88%, indicating their dynamic characteristics. MTNZPy also exhibited a similar organelle-targeting. This work also paved a new avenue for research on diseases caused by lysosome-dependent variation.

The ability of lysosomes to hydrolyze greatly impedes the ability of nanomaterials for drug delivery, therefore, how the materials could escape from lysosome becomes a concern that attracted much attention. In order to achieve this goal, the core-shell SNA was finally constructed from nanoparticles with AIE-photosensitizers and Bcl-2 antisense oligonucleotides(OSAs)[Fig.7(A)][69]. Upon driving by light, large amounts of ROS were generated due to the AIE-photosensitizers, which could destroy the structure of lysosome and facilitate the SNA to escape from lysosome. Benefiting from a typical D-A-D structure, the AIE-photosensitizer possessed far-red emission and effective $^1O_2$ generation under the irradiation of white light. In addition, Inspired by the classic clicking reaction, the AIE-photosensitizer with terminal acetylene was firstly linked with PEG to constructed a new polymer, with a $-N_3$ group. And then, assembled nanoparticles with $-N_3$ conjugated with an antisense OSA to form the SNA, which could be capable of targeting Bcl-2 mRNA. The confocal images testified that the

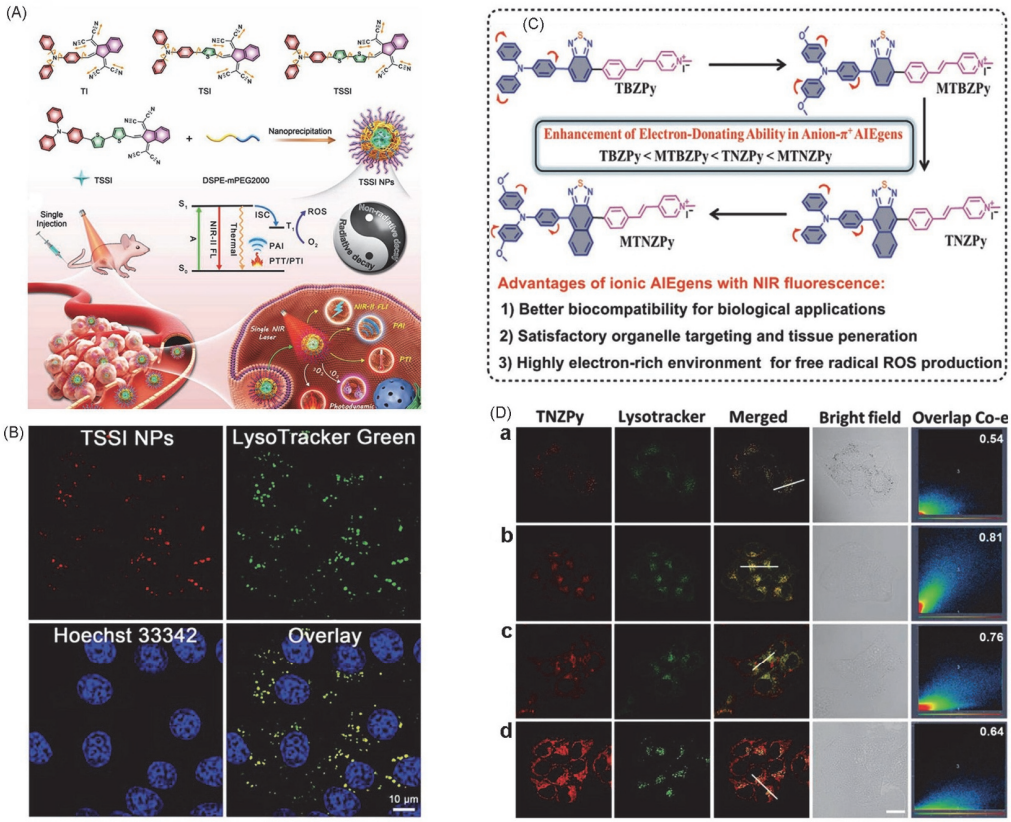


**Fig.6 Chemical structures, preparation and multi-modal theranostics of TI, TSI and TSSI(A), CLSM images of 4T1 cells after incubation with TSSI NPs for 3 h(B), molecular structures of TBZPy, MTBZPy, TNZPy, and MTNZPy(C) and confocal images of HeLa cells incubated with TNZPy for 4, 6, 12, and 24 h(a—d), respectively(co-localization with Lysotracker green)(D)**

(A, B) Reprinted with permission from Ref.[66], Copyright 2020, Wiley-VCH. (C, D) Reprinted with permission from Ref.[68], Copyright 2020, Wiley-VCH.


https://doi.org/10.1007/s40242-021-0430-1

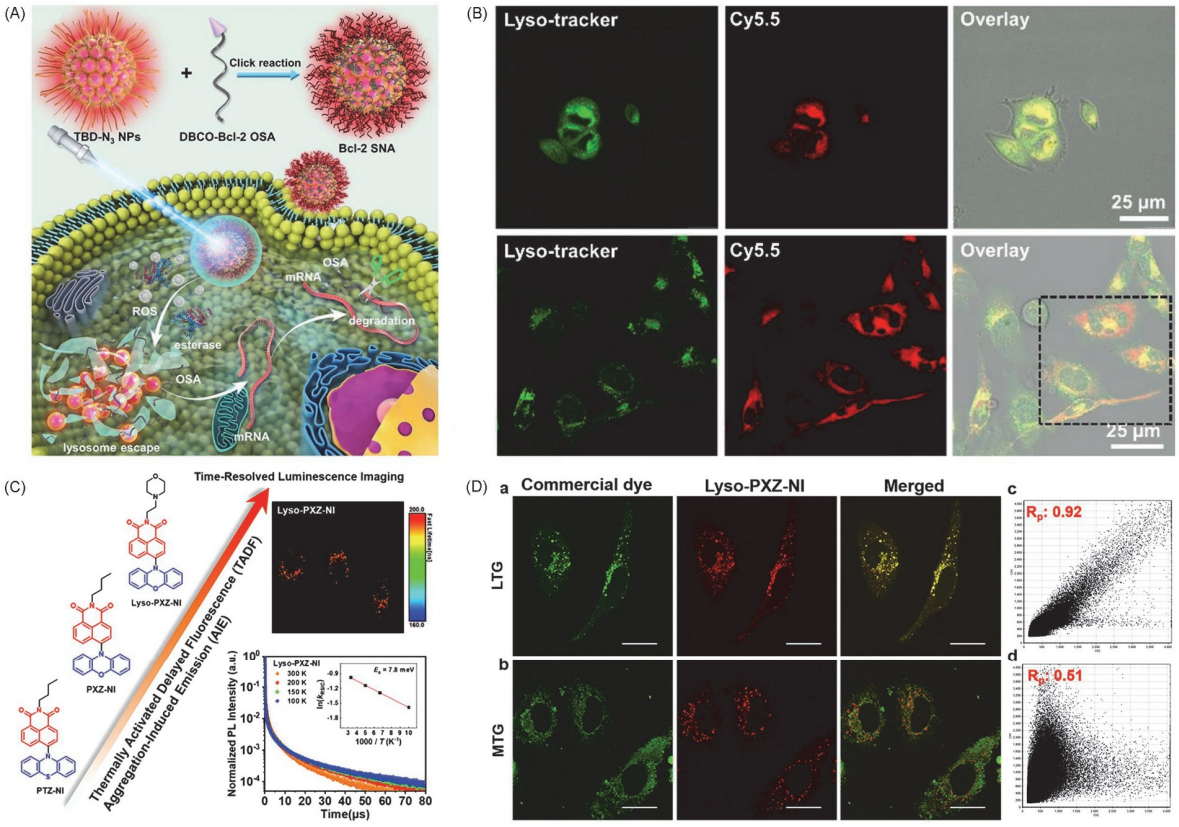


**Fig.7 Schematic illustration of the preparation of Bcl-2 SNA based on an AIE-active photosensitizer(the generation of ROS in the lysosome could rupture its structure, resulting in degradation of Bcl-2 mRNA and improve the PDT effect, A), confocal imaging of HeLa cells co-localized with lysosome tracker(green) and Cy5.5 labeled Bcl-2 SNA(red) under dark and light irradiation, respectively(B), molecular structures of TADF organic materials, confocal images and fluorescent images of HeLa cells treated with Lyso-PXZ-NI with temperature-dependent TRPL signals and Arrhenius plots of Lyso-PXZ-NI doped into PMMA films(C) and fluorescent images of HeLa cells incubated with Lyso-PXZ-NI and LTG(a) or MTG(b), and fluorescence intensity correlation of Lyso-PXZ-NI with LTG(c) and MTG(d)(D)**

(A, B) Reprinted with permission from Ref.[69], Copyright 2020, Wiley-VCH. (C, D) Reprinted with permission from Ref.[70], Copyright 2020, American Chemical Society.

majority of double-stranded DNA with Cy5.5 could escape from both endosomes and lysosomes[Fig.7(B)].

Recently, thermally activated delayed fluorescence(TADF) material with long-lived fluorescence is regarded as one of good materials for time-resolved biological imaging. Yoon and co-workers[70] designed and synthesized a kind of new organic TADF materials with long lifetime for time-resolved fluorescence imaging in cancer cells. The Lyso-PXZ-NI luminophore could be able to target the lysosomes[Fig.7(C)], resulted from the introduction of 2-morpholine moiety to act as the lysosome-targeted group. The maximum absorption of PXZ-NI was located at 500 nm and that of PTZ-NI was at 450 nm. Additionally, Lyso-PXZ-NI has almost similar optical properties including absorption and emission with PXZ-NI. As shown in Fig.7(D), Lyso-PXZ-NI was found to overlap well with commercial LysoTracker green in co-staining experiments, which also indicates their selective targeting toward lysosomes. Cellular experiments also confirmed the good cell permeability and biocompatibility of all the TADF materials. This study indicates that combining the chemo-therapeutic drugs and photosensitive, AIEgens will provide great opportunities for the improvement of synergistic therapeutic effects. Chemotherapeutics break the limitation of superficial penetration of light, while phototherapeutics enhance the activities of drugs by overcoming the drug-resistance.

## 6 Mitochondria

Mitochondria is one of the most important subcellular organelles. It is the structure for producing ATP energy and the main place to carry out aerobic respiration in cells, which is so-called “power house”. Mitochondria can not only provide energy, but also produce ROS, regulate transcription and control cell death. Many diseases are related to the dynamics and morphology of mitochondria. Protein mutations often lead to many diseases, such as neurodegeneration. Therefore, further development of novel mitochondrial fluorescence staining is of great significance for monitoring these processes, studying their


https://doi.org/10.1007/s40242-021-0430-1

biological functions and understanding their mechanisms.

Recently, mitochondrial-targeted PDT has attracted much attention due to its better therapeutic effect. However, fluorescence imaging-guided PDT is often limited by two aspect, namely the ACQ effect suffered from the conventional photosensitizers(PSs) and the severe hypoxia in solid tumors. To overcome these problems, a strong ICT effect was achieved in anion-π AIEgens to suppress nonradiative internal conversion and boost free radical generation by the efficient capture of an electron from the excited AIE-PSs[71]. Both TNZPy and MTNZPy can target to mitochondria and lysosomes. The author investigated the therapeutic mechanism and found that the integrity of mitochondrial and lysosomes organelles was destroyed by the free radical ROS after light triggering, subsequently leading to cell apoptosis. Another excellent work to overcome hypoxia in solid tumors is also reported[72]. The hybrid nanovesicles DES by tumor-exocytosed EXO/AIEgen were developed by an electroporation method to penetrate tumors *in vivo*. The use of Dexamethasone normalized vascular function and reduced hypoxia in the tumor, thereby leading to effectively inhibition of the growth of the tumor.

Considering the advantages of black phosphorus(BP) nanomaterials and AIE PSs in tumor treatment, a new multifunctional theranostic nanoplatform was constructed by marrying AIE-PSs with BP nanosheets[Fig.8(A)][73]. The positively charged water-soluble AIE PS(NH2-PEG-TTPy) was easily synthesized through three steps reactions, and subsequently added to BP nanosheets surface through electrostatic interaction. The co-localization experiment showed that BP@PEG-TTPy first came into lysosomes, then the acidic lysosomal environment enabled the partial protonation of the amine groups in $NH_2$-PEG-TTPy, which led to the separation of BP nanosheets and $NH_2$-PEG-TTPy. Subsequently the $NH_2$-PEG-TTPy was released from the lysosomes due to the proton sponge effect. Finally, these positively charged $NH_2$-PEG-TTPy targeted to mitochondria through electrostatic interaction [Fig.8(B)]. The physiological and biocompatible stability of the BP nanosheets was improved in the hybrid nanomaterial. Moreover, the PDT capability and strong NIR fluorescence emission enabled the good performance in FLI-PTI dual imaging-guided PDT-PTT phototherapy in cancer treatment.

Kim and his colleagues[74] found Kaleidolizine(KIz) as a new color molecular platform for AIEgens[Fig.9(A)]. The emission wavelength of the Klz system can be systematically turned from 455 nm to 564 nm by changing the indolizine core's substituents. The fluorescence of KIz series is fairly weak in solution but very high in the solid state. The fluorescence intensity dramatically increased up to 120-fold with the increase of the water fraction. In addition, a mitochondrial-targeted bioprobe TPP-Klz was successfully constructed by conjugating the TPP moiety to KIz, which revealed the great potential of KIz as a versatile molecular platform for the generation of AIE fluorogenic probes[Fig.9(B)]. Different from the traditional transformation from ACQ-to-AIE molecular, TBP-b-TPA achieved highly bright fluorescence emission in solid state through regioisomerization with tuning the packing mode of molecules[75]. The Pearson correlation coefficient of TBP-b-TPA overlapped with Mito Tracker green is up to 0.903, which showed that TBP-b-TPA has an excellent mitochondrial targeting ability.

To solve the small Stokes shift and aggregation caused quenching(ACQ) effect suffered in many typical molecular rotors, Hong and co-workers[76] have recently developed a set of novel red emissive molecular rotors containing cationic *α*-cyanostil-bene, namely ACS, ASCP, and new derivatives of ASCP[Fig.9(C) and (D)]. ASCP series have a better AIE property

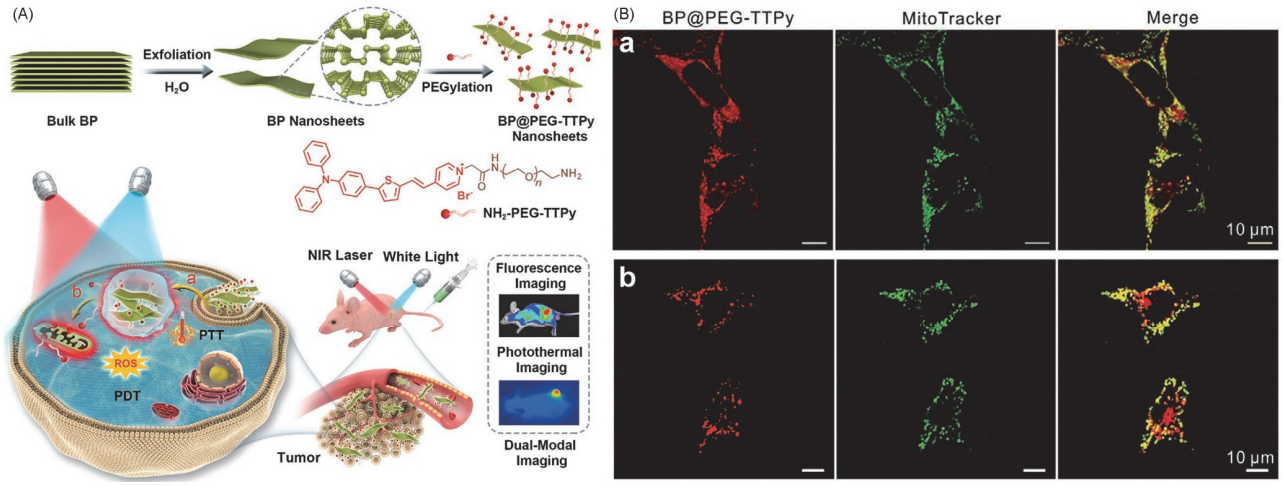


**Fig.8 Schematic presentation of the construction of BP@PEG-TTPy nanosheets and the representation of imaging-guided synergistic PDT-PTT by the materials(A) and confocal imaging in mitochondria in the absence (a) and presence(b) of light irradiation by irradiation of white light and 808 nm laser(B)**

Reprinted with permission from Ref.[73], Copyright 2020, Wiley-VCH.

than ASC due to the additional phenyl ring bridge and show specificity to mitochondria. Moreover, the cell uptake and retention of ASCP can be achieved *via* changing the substituents on the pyridinium. Although mitochondria-targeted AIE PSs show great potential in the field of cancer therapy due to its high ROS generation capability, the ultrastructural changes of mitochondria induced by AIE PSs during PDT process have rarely been discovered, which is beneficial for revealing the therapeutic mechanism. Recently, Li and co-workers[77] reported a mitochondria-targeted AIE PSs with self-monitoring capacity, namely TTVPHE. It can not only precisely control ROS release under the light irradiation, but also *in situ* monitor the therapeutic process by translocation from the damaged mitochondria to nucleus membrane. With the aid of the high-resolution transmission electron microscopy(HR-TEM), the ultrastructure of damaged mitochondria was characterized.

Although mitochondrial-targeted PDT using AIE PSs has been made great progress in recent years, there are several factors that limit the PDT therapeutic efficiency. For example, overexpression of Bcl-2 protein in cancer cells enhanced the antiapoptotic, antioxidant and capability of cells, which reduced the effect of PDT. To address this issue, the synthetic AIEgen-lipid molecules were labeled with the isolated bioactive Mito to fabricate the AIE-PS-engineered Mito by Liu and co-workers [Fig.9(E)][78]. After internalization into cancer cells, the fluorescence of free AIEgen-lipid was evenly distributed in the cytoplasm uniformly, while a large number of green spots appeared in the cytoplasm of cancer cells treated with Mito-AIEgen-lipid[Fig.9(F) and (G)]. The Mito-AIEgen-lipid established a more efficient and normal metabolic pathway for ATP synthesis to replace aerobic glycolysis *via* oxidative phosphorylation. In addition, the PDT effect of Mito-AIEgen-lipid could be enhanced dramatically under light irradiation by up-regulating the expression of apoptosis-inducing factor and down-regulating the apoptosis-antagonizing protein to reactivate the apoptotic pathway.

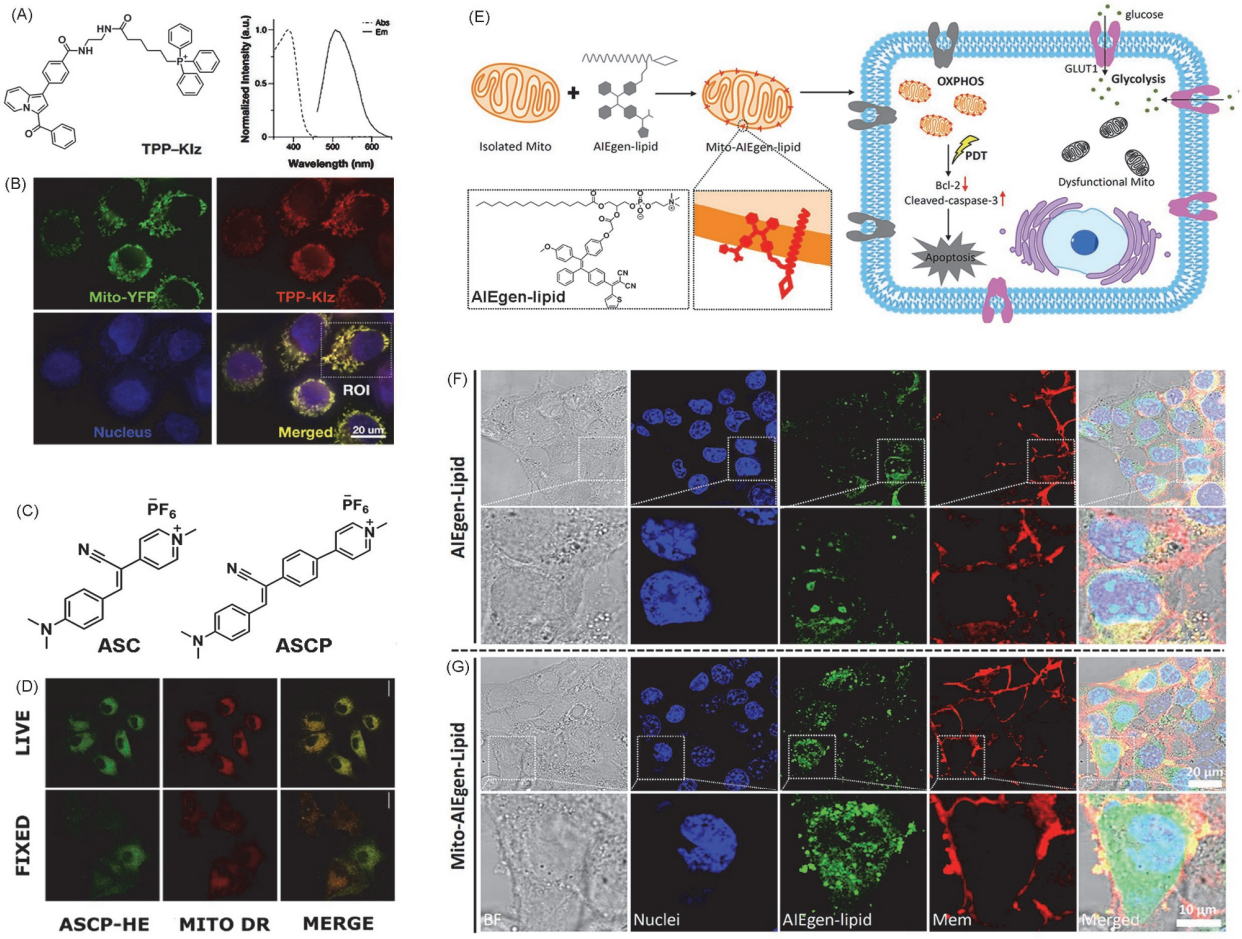


**Fig.9 Molecular structures of TPP-Klz and its absorption and emission spectra(A), confocal imaging of Chang liver cells co-staining by protein(Mito-YFP) and TPP–Klz, Hoechst dye, respectively(B), torsional angles of ASC and ASCP(C), mitochondrial colocalization of ASCP-HE stained A549 cells and for visualization of mitochondria(D), schematics of AIEgen-modified mitochondria and the rescuing of energy metabolism(E), the experiments of cellular uptake of AIEgen-lipid(F) and Mito-AIEgen-lipid(G)**

(A, B) Reprinted with permission from Ref.[74], Copyright 2020, American Chemical Society; (C, D) reprinted with permission from Ref.[76], Copyright 2020, American Chemical Society; (E—G) reprinted with permission from Ref.[78], Copyright 2020, American Chemical Society.


https://doi.org/10.1007/s40242-021-0430-1

## 7 Cytoplasm

Effective cell imaging and high-performance long-term cell tracking in a non-intrusive and real-time way are able to provide critical information on the physiological process of actively migrating cells, which is greatly significant for precise cancer diagnosis and therapy, and also for the monitoring of biological processes. By virtue of their unique advantages including good biocompatibility, high fluorescence brightness, large Stokes shift, and excellent photostability, AIEgens have been proved to exhibit outstanding performances in cell imaging and long-term cell tracking[79]. For instance, a water-soluble AIEgen BSPO-TPE reported by Tang *et al*. in 2017[80] was recently demonstrated to be able to light up the cytoplasm of healthy and living mammalian cells, and the fluorescence signal can still be observed after 48 h and even in the daughter cells at 24 h post-staining. It was speculated that the fluorescence comes from BSPO-TPE bound to the proteins of the subcellular organelles or cytoskeleton in living cells because BSPO-TPE has early been proved to likely bind to proteins. With cytoplasm imaging ability and high photostability, BSPO-TPE showed great possibility in live cell tracking.

The preparation of AIE nanoparticles smaller than 10 nm for the purpose of more efficient cellular uptake has been a challenging task for a long time. Very recently, Jiang *et al*.[81] developed a robust platform, which could be used to assemble organic AIE particles less than 10 nm(defined as AIE QDs). Compared with the normal AIE dots(>25 nm) fabricated *via* nanoprecipitation method, the synthesized AIE QDs(<10 nm) by means of microfluidic method exhibit more efficient cell internalization and cytoplasm imaging ability without the aid of any membrane-penetrating peptides and targeting molecules. They also demonstrated that the sub-10 nm AIE QDs can largely evade the capture of the reticuloendothelial system and liver, and provide high contrast tumor imaging with the aid of NIR-II AIEgen. Fluorescent polymer dots(Pdots), particularly the stimuli-responsive ones, are emerging as a new class of high-efficiency fluorophores for cell imaging owing to their high emissivity, excellent fluorescence brightness and good compatibility[82]. On basis of this awareness, Chi *et al*.[83] synthesized a three diblock copolymer(PTPEE-PN*n*s) with both AIE features and thermos-responsive characteristics *via* reversible addition-fragmentation chain transfer(RAFT) polymerization[Fig.10(A)]. Thanks to their amphiphilic properties, PTPEE-PN*n* copolymers are likely to form micelles in an aqueous solution, and the particle size of which could be affected by the fabrication method. It was demonstrated that the particle size and size distribution of PTPEE-PN2 micelles prepared by the "dialysis" method presented relatively small and narrow. Owing to the employment of the thermal-responsive group(NIPAM), the obtained copolymer displayed a distinct phase change in the temperature range of 24—32 °C, leading to the size change of the micelles. Furthermore, PTPEE-PN2-M2 micelles could exhibit strong blue fluorescence in the cytoplasm of U2OS cells[Fig.10(B)]. With excellent particle stability and good biocompatibility, PTPEE-PN2-M2 micelles could be utilized as an efficient fluorescent probe for cytoplasm imaging. In addition, Lai *et al*.[84] synthesized a succession of stimuli-responsive dual-color Pdots with AIE properties, namely 4s-TPE-PCL-b-PNIPAM-Eu(III)(TPNE), 4s-TPE-PCL-b-PAA-Eu(III)(TPAE) and 4s-TPE-PCL-b-PVP-Eu(III)(TPVE). These Pdots were self-assembled from three amphiphilic block copolymers, which were synthesized by free-radical polymerization using a macroazoinitiator consisting of AIE fluorophore tetrapheny-lethene(TPE), poly($\varepsilon$-caprolactone) (PCL) group and azo segment, respectively. The resulted TPNE, TPAE and TPVE Pdots are demonstrated to show extremely small diameters(5 nm), good water-solubility and monodispersity, thermo-tunable and pH-dependent fluorescence property, outstanding photostability as well as good biocompatibility. All these Pdots could effectively enter and be located in the cytoplasm of cells. Since the Pdots exhibited two emission peaks at 430 and 615 nm, separately, the fluorescence signal in cytoplasm could be detected in two different channels by altering the excitation wavelength, indicating their potential applications in fluorescence probing and multicolour bioimaging.

Multi-modality theranostics that possesses both diagnostic and therapeutic functions has been considered as a powerful weapon for the precise diagnosis and efficient treatment of cancer[85]. In terms of multimodal imaging-guided cancer therapy, Lee *et al*.[86] reported a single-photomolecular nanothera-nostics based on conjugated oligomer nanoparticles (IT-S NPs), which was demonstrated to exhibit NIR emission and high photothermal conversion efficiency(PCE) of 72.3% as well as excellent photothermal stability[Fig.10(C)]. *In vitro* experiments showed that IT-S NPs could be internalized into the cytoplasm rather than the nuclei, giving apparent NIR fluorescence signals. After uptaken by the cells, IT-S NPs exhibit concentration-dependent cytotoxicity after 635 nm laser irradiation for 5 min, owing to the efficient photothermal ablation capacity. By virtue of their NIR emission and high PCE, IT-S NPs successfully achieved dual-mode NIR fluorescence imaging(FLI) and photoacoustic imaging(PAI) *in vivo*. The *in vivo* anti-tumor experiments demonstrated that the tumor could be completely ablated by virtue of the photothermal ablation (PTA) perfor-mance of IT-S NPs with no obvious recurrence observed. In order to further improve the diagnosis and antitumor response of multi-modality theranostics, Tang *et al*.[87] designed and synthesized a string of zwitterionic AIEgens(ITB, ITT, BITB and BITT) for NIR-II fluorescence imaging-guided


https://doi.org/10.1007/s40242-021-0430-1

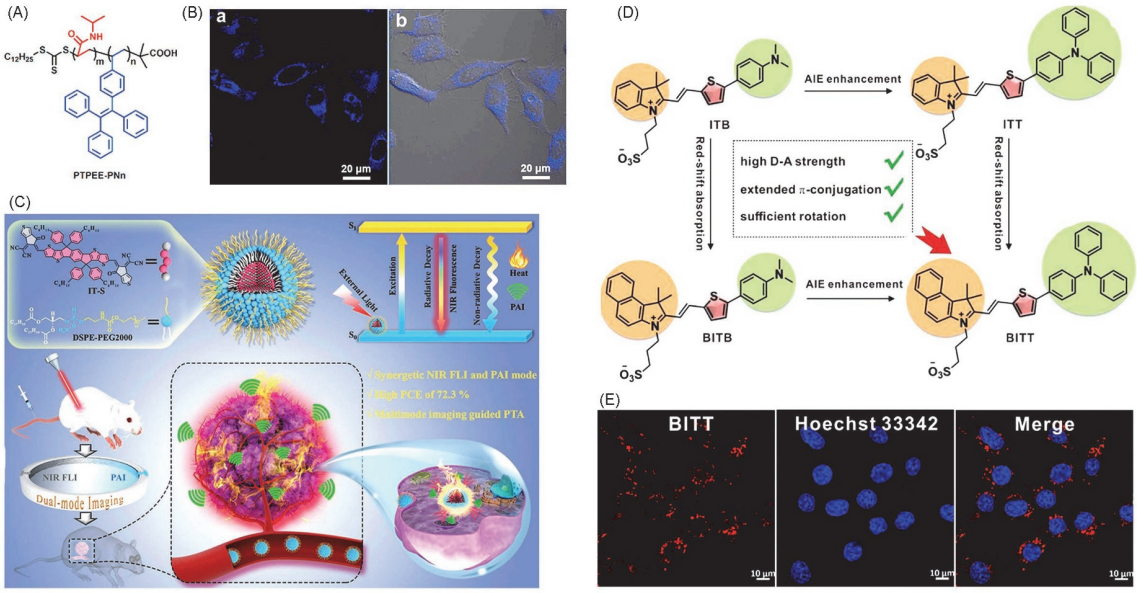


**Fig.10 Structure of PTPEE-PN*n*(A), CLSM images(a. fluorescence image; b. merged image and bright field) of U2OS cells incubated with PTPEE-PN2-M2(B), schematic representation of single-photomolecular nanotheranostic system(C), designing and synthesizing of zwitterionic AIEgens(named as ITB, ITT, BITB and BITT)(D) and confocal images of 4T1 cells co-localizing with BITT and Hoechst 33342(E)**

(A, B) Reprinted with permission from Ref.[83], Copyright 2021, Elsevier Publishing Group; (C) reprinted with permission from Ref.[86], Copyright 2020, Wiley-VCH; (D, E) reprinted with permission from Ref.[87], Copyright 2020, Wiley-VCH.

PDT-PTT synergistic phototherapy[Fig.10(D)]. After being fabricated into AIE dots through nanoprecipitation, BITT dots were shown to mainly localize in the cytoplasm and exhibited bright red fluorescence inside 4T1 cell[Fig.10(E)]. By taking full advantages of their emission in NIR-II region, efficient ROS generation efficiency and high PCE, BITT dots provided excellent performances in NIR-II FLI guided tumor elimination on 4T1 tumor-bearing mice.

Imaging of hypoxia *in vivo* could significantly benefit to the accurate cancer diagnosis and assessment of therapeutic effect[88]. Aiming to detect and image hypoxia as well as exert therapeutic effect in the hypoxic tumor, Stang *et al*.[89] reported a kind of supramolecular coordination complexes($Pt^{II}$ metallacage) for *in vivo* hypoxia imaging as well as chemotherapy. Therein, the $Pt^{II}$ metallacage was endowed with oxygen-responsive red phosphorescence and steady fluorescence owing to the integration of phosphorescent ligand $Pt^{II}$-meso-tetra(4-carboxyphenyl)porphine and blue fluorophore anthracene. The as-prepared metallacage-loaded nanoparticles(MNPs) are proven to mainly distribute in the cytoplasm and exhibit green and blue emission under normoxia condition, while both green/blue fluorescence and red phosphorescence were observed from the cytoplasm under the hypoxia condition, providing a more reliable protocol for hypoxia detection and imaging by taking advantage of the red/blue ratio. Furthermore, *in vivo* experiments also demonstrated that MNPs showed great potentials in cancer theranostics involving tumor hypoxia imaging and chemotherapy.

There are also large amounts of intermediates or biomarkers in the cytoplasm. For example, as a tripeptide compound, Glutathione(GSH) commonly exists in cells and is always overexpressed when the cells are diseased. You and coauthors[90] reported an AIEgen as the DNA probe in living cells, which can track the reduced thiol compounds(GSH) in living cells. The added amounts of $H_2S$ result in the increased tumorigenesis in many cancers. Tian and coworkers[91] developed two probes to $H_2S$ for targeted cancer imaging, with aggregation enhanced responsiveness. Tang and coauthors[92] also synthesized an AIE-active detector for HClO in living cells. Typically, Tang, Cao and co-authors[93] also developed the fluorescent probe for anthrax spore biomarker, which was self-assembled from the AIE-based $Tb^{3+}$ complex. Zhu and Li *et al*.[94] reported the AIE-active bioprobes for visualization of protein amyloid fibrillation from hen egg white lysozyme, which is one of the important indicators for degenerative diseases, such as Parkinson's disease, type II diabetes.

## 8 Conclusions and Perspectives

Herein, very recent advances in targeted imaging toward subcellular organelles, based on well-designed AIEgens, were summarized and presented in this review. With the fast development of techniques for designing and synthesizing AIE-active compounds, a variety of bioprobes with AIE effect have been reported to achieve targeted imaging and integrated theranostics at the cellular level so far. In particular, the AIE


https://doi.org/10.1007/s40242-021-0430-1

bioprobes for subcellular organelles, such as nucleus, cell membranes, lipid droplets, endoplasmic reticulum, lysosomes, mitochondria, etc., have also been widely explored *via* elaborating designing and syntheses. In contrast to ACQ dyes, AIEgens provide us the feasible strategies to precisely study the morphologies, functions and interactions of organelles, promoting the research progress of high-resolution imaging for specific detection. Furthermore, the visualization of organelles with AIE bioprobes also provides us the guidance for disease treatments, with which we can gain a deep understanding of the pathogenesis and control the therapeutic process in the course of treatments. However, the AIEgens as the bioprobes for tracking of subcellular structures are still in infancy, because of the sophisticated architectures and substances within cells. On the other hand, the typical features of subcellular organelles should be further explicit, which will be helpful for the design and synthesis of more specific bioprobes with AIE properties.

During the past two decades, we have witnessed the rapid developments of AIEgens and their applications in the fields of biological medicines and accurate theranostics. However, there are still some challenges and bottlenecks that need to be solved due to the limitation of techniques, even though extensive investigations have been tried and reported. First of all, the deep understanding of the subcellular organelles will help us make better designing of the AIE bioprobes. Special biomarkers for each organelle should be better classified and explicit. Thus, better communications with other biological disciplines should be established to realize the selective targeting imaging for each organelle. Secondly, the targeted-imaging for lysosomes and mitochondria have been largely reported, but the AIE probes for ER, especially for Golgi apparatus have seldom been reported. Considering their vital roles in cells, much more attentions should be paid to these kinds of organelles. Finally, the AIEgens with the ability of multi-modal imaging are of great significance and should be developed, which will play a crucial role in early diagnosis of diseases. Meanwhile, the synergistic imaging and automatic switching of imaging in different organelles will help us understand more about the mechanism for life activities, metabolism and pathogenesis.

Benefiting from the superior advantages of AIE bioprobes and the great potentials, it can be envisaged that cracking achievements would be made for early diagnosis and therapeutics of miscellaneous diseases.

## Acknowledgements

This work was supported by the Developmental Fund for Science and Technology of Shenzhen, China(Nos.JCYJ20190808153415062, JCYJ20190808121417291), the China Postdoctoral Science Foundation(No.2020M672791), the National Natural Science Foundation of China(Nos.21801169, 52003164), and the Natural Science Foundation for Distinguished Young Scholars of Guangdong Province, China(No.2020B1515020011).

## Availability of Data and Materials

All data generated or analyzed during this study are included in this published article and its supplementary information files.

## Conflicts of Interest

The authors declare no conflicts of interest.

## References

[1] Yang J., Dai J., Wang Q., Cheng Y., Guo J., Zhao Z., Hong Y., Lou X., Xia F., *Angew. Chem. Int. Ed.*, **2020**, *59*, 20405
[2] Singh H., Lee H. W., Heo C. H., Byun J. W., Sarkar A. R., Kim H. M., *Chem. Commun.*, **2015**, *51*, 12099
[3] Ayoubi-Joshaghani M. H., Seidi K., Azizi M., Jaymand M., Javaheri T., Jahanban-Esfahlan R., Hamblin M. R., *Adv. Funct. Mater.*, **2020**, *30*(45), 2004098
[4] Li L., Yang Z., Chen X., *Acc. Chem. Res.*, **2020**, *53*(10), 2044
[5] Li J., Wang J., Li H., Song N., Wang D., Tang B. Z., *Chem. Soc. Rev.*, **2020**, *49*, 1144.
[6] Chen J., Liu H., Yang L., Jiang J., Bi G., Zhang G., Li G., Chen X., *ACS Med. Chem. Lett.*, **2019**, *10*(6), 954
[7] Situ B., Ye X., Zhao Q., Mai L., Huang Y., Wang S., Chen J., Li B., He B., Zhang Y., Zou J., Tang B. Z., Pan X., Zheng L., *Adv. Sci.*, **2020**, *7*(4), 1902760
[8] Yu K., Pan J., Husamelden E., Zhang H., He Q., Wei Y., Tian M., *Chem. Asian. J.*, **2020**, *15*(23), 3942
[9] Brewer T. F., Chang C. J., *J Am. Chem. Soc.*, **2015**, *137*(34), 10886
[10] Kamiya M., Asanuma D., Kuranaga E., Takeishi A., Sakabe M., Miura M., Nagano T., Urano Y., *J. Am. Chem. Soc.*, **2011**, *133*(33), 12960
[11] Kowada T., Watanabe T., Amagai Y., Liu R., Yamada M., Takahashi H., Matsui T., Inaba K., Mizukami S., *Cell. Chem. Biol.*, **2020**, *27*(12), 1521
[12] Zhou Y., Hua J., Tang B. Z., Tang Y., *Sci. Chin. Chem.*, **2019**, *62*(10), 1312
[13] Li C., Chen G., Zhang Y., Wu F., Wang Q., *J. Am. Chem. Soc.*, **2020**, *142*(35), 14789
[14] Won M., Li M., Kim H. S., Liu P., Koo S., Son S., Seo J. H., Kim J. S., *Coord. Chem. Rev.*, **2021**, *426*, 213608
[15] Xin H., Li Y., Liu Y. C., Zhang Y., Xiao Y. F., Li B., *Adv. Mater.*, **2020**, *32*(37), e2001994
[16] Ding S., Hong Y., *Chem. Soc. Rev.*, **2020**, *49*, 8354
[17] Banik D., Manna S. K., Mahapatra A. K., *Spectrochim Acta A Mol. Biomol. Spectrosc.*, **2021**, *246*, 119047
[18] Zhao Z., Zhang H., Lam J. W. Y., Tang B. Z., *Angew. Chem., Int. Ed.*, **2020**, *59*, 9888
[19] Luo J., Xie Z., Lam J. W. Y., Cheng L., Chen H., Qiu C., Kwok H. S., Zhan X., Liu Y., Zhu D., Tang B. Z., *Chem. Commun.*, **2001**, 1740
[20] Xu W., Wang D., Tang B. Z., *Angew. Chem. Int. Ed.,* **2020**, doi: 10.1002/anie.202005899
[21] Kang M., Zhang Z., Song N., Li M., Sun P., Chen X., Wang D., Tang B. Z., *Aggregate,* **2020**, *1*(1), 80
[22] Xu W., Lee M. M. S., Nie J.-J., Zhang Z., Kwok R. T. K., Lam J. W. Y., Xu F.-J., Wang D., Tang B. Z., *Angew. Chem. Int. Ed.,* **2020**, *59*, 9610
[23] Yan D., Wu Q., Wang D., Tang B. Z., *Angew. Chem. Int. Ed.,* **2020**, doi: 10.1002/anie.202006191
[24] Zhang H., Zhao Z., Turley A. T., Wang L., McGonigal P. R., Tu Y., Li Y., Wang Z., Kwok R. T. K., Lam J. W. Y., Tang B. Z., *Adv. Mater.*, **2020**, *32*(36), e2001457
[25] Jiang G., Li C., Liu X., Chen Q., Li X., Gu X., Zhang P., Lai Q., Wang J., *Adv. Opt. Mater.,* **2020**, *8*(20), 2001119
[26] Qi G., Hu F., Chong K. C., Wu M., Gan Y. H., Liu B., *Adv. Funct. Mater.,* **2020**, *30*(31), 2001338
[27] Ma X., Wang J., Tian H., *Acc. Chem. Res.,* **2019**, *52*(8), 738
[28] Li J., Zhang Y., Wang P., Yu L., An J., Deng G., Sun Y., Seung Kim J., *Coord. Chem. Rev.*, **2021**, *427*, 213559
[29] Roy E., Nagar A., Chaudhary S., Pal S., *Indust. & Engin. Chem. Res.*, **2020**, *59*(23), 10721
[30] Wang D., Tang B. Z., *Acc. Chem. Res.*, **2019**, *52*(9), 2559
[31] Wu H., Huang W., Zhou X., Min Y., *Front. Immunol.*, **2020**, *11*, 575816
[32] Ghareeb H., Metanis N., *Chem. Eur. J.,* **2020**, *26*(45), 10175
[33] Liu H., Xiong L.-H., Kwok R. T. K., He X., Lam J. W. Y., Tang B. Z., *Adv. Opt. Mater.,* **2020**, *8*(14), 2000162
[34] Song N., Zhang Z., Liu P., Yang Y. W., Wang L., Wang D., Tang B. Z., *Adv. Mater.*, **2020**, e2004208
[35] Wang J., Li J., Wang L., Han T., Wang D., Tang B. Z., *ACS Appl. Poly. Mater.*, **2020**, *2*(10), 4306
[36] Kalva N., Uthaman S., Jang E. H., Augustine R., Jeon S. H., Huh K. M., Park I.-K., Kim I., *Dyes and Pigments*, **2020**, doi: 10.1016/j.dyepig.2020.

108975
[37] Ma L. L., Tang Q., Liu M. X., Liu X. Y., Liu J. Y., Lu Z. L., Gao Y. G., Wang R., *ACS Appl. Mater. Interfaces*, **2020**, *12*(36), 40094
[38] Wang L., Urbas A. M., Li Q., *Adv. Mater.*, **2020**, *32*(41), e1801335
[39] Hong Y., Chen S., Leung C. W., Lam J. W., Tang B. Z., *Chem. Asian. J.*, **2013**, *8*(8), 1806
[40] Xu X., Yan S., Zhou Y., Huang R., Chen Y., Wang J., Weng X., Zhou X., *Bioorg. Med. Chem. Lett.*, **2014**, *24*(7), 1654
[41] Ma H., Yang M., Zhang C., Ma Y., Qin Y., Lei Z., Chang L., Lei L., Wang T., Yang Y., *J. Mater. Chem. B*, **2017**, *5*(43), 8525
[42] Zhang T., Li Y., Zheng Z., Ye R., Zhang Y., Kwok R. T. K., Lam J. W. Y., Tang B. Z., *J. Am. Chem. Soc.*, **2019**, *141*(14), 5612
[43] Pieszka M., Han S., Volkmann C., Graf R., Lieberwirth I., Landfester K., Ng D. Y. W., Weil T., *J. Am. Chem. Soc.*, **2020**, *142*(37), 15780
[44] Yu C. Y. Y., Zhang W., Kwok R. T. K., Leung C. W. T., Lam J. W. Y., Tang B. Z., *J. Mater. Chem. B*, **2016**, *4*, 2614
[45] Liang J., Feng G., Kwok R. T. K., Ding D., Tang B., Liu B., *Sci. Chin. Chem.*, **2016**, *59*, 53
[46] Wu M.-Y., Leung J.-K., Liu L., Kam C., Chan K. Y. K., Li R. A., Feng S., Chen S., *Angew. Chem. Int. Ed.*, **2019**, *59*, 10327
[47] Ma L., Tang Q., Liu M.-X., Liu X.-Y. Liu, J.-Y., Lu Z.-L., Gao Y.-G., Wang R., *ACS Appl. Mater. Interfaces*, **2020**, *12*, 40094
[48] Sezgin E., Levental I., Mayor S., Eggeling C., *Nat. Rev. Mol. Cell Biol.*, **2017**, *18*, 361
[49] Zhang W., Huang Y., Chen Y., Zhao E., Hong Y., Chen S., Lam J. W. Y., Chen Y., Hou J., Tang B. Z., *ACS Appl. Mater. Interfaces*, **2019**, *11*, 10567
[50] Zheng Y., Ding Y., Ren J., Xiang Y., Shuai Z., Tong A., *Anal. Chem.*, **2020**, *92*(21), 14494
[51] Dong Q.-J., Cai Z.-B., Ding L., Luo P.-H., He Q.-J., Li S.-L., Chen L.-J., Ye Q., Tian Y.-P., *Dyes and Pigments*, **2021**, *185*, 108849
[52] Komatsu T., Kyo E., Ishii H., Tsuchikama K., Yamaguchi A., Ueno T., Hanaoka K., Urano Y., *J. Am. Chem. Soc.*, **2020**, *142*(37), 15644
[53] Li M., Zhang W., Wang B., Gao Y., Song Z., Zheng Q. C., *Nanomed.*, **2016**, *11*, 5645
[54] Delcanale P., Porciani D., Pujals S., Jurkevich A., Chetrusca A., Tawiah K. D., Burke D. H., Albertazzi L., *Angew. Chem. Int. Ed.*, **2020**, *59*, 18546
[55] Gao M., Tang B. Z., *Coordin. Chem. Rev.*, **2020**, *402*, 213076
[56] Shi H., Liu J., Geng J., Tang B. Z., Liu B., *J. Am. Chem. Soc.*, **2012**,*134*, 9569
[57] Duan Y., Wu M., Hu D., Pan Y., Hu F., Liu X., Thakor N., Ng W. H., Liu X., Sheng Z., Zheng H., Liu B., *Adv. Funct. Mater.*, **2020**, *30*(38), 2004346
[58] Xie Y.-Y., Zhang Y.-W., Liu X.-Z., Ma X.-F., Qin X.-T., Jia S.-R., Zhong C., *Chem. Engineer. J.*, **2020**, 10.1016/j.cej.2020.127542
[59] Zhang F., Li Z., Liu Y., Yang B., Qiao H., Chai Ji., Wen G., Liu B., *J. Mater. Chem. B*, **2020**, *8*(41), 9533
[60] Sodre E. R., Guido B. C., de Souza P. E. N., Machado D. F. S., Carvalho-Silva V. H., Chaker J. A., Gatto C. C., Correa J. R., Fernandes T. A., Neto B. A. D., *J. Org. Chem.*, **2020**, *85*(19), 12614
[61] Reza A. H. M. M., Zhou Y., Tavakoli J., Tang Y., Qin J., *Mater. Chem. Front.*, **2021,** doi: 10.1039/D0QM00621A
[62] Ling X., Huang L., Li Y., Wan Q., Wang Z., Qin A., Gao M., Tang B. Z., *Mater. Horiz.*, **2020**, *7*, 2696
[63] Alam P., He W., Leung N. L. C., Ma C., Kwok R. T. K., Lam J. W. Y., Sung H. H. Y., Williams I. D., Wong K. S., Tang B. Z., *Adv. Funct. Mater.*, **2020**, *30*(10), 1909268
[64] Zhu Z., Wang Q., Liao H., Liu M., Liu Z., Zhang Y., Zhu W.-H., *Nat. Sci. Rev.*, **2020**, doi: 10.1093/nsr/nwaa198/5899762
[65] Yang M., Deng J., Su H., Gu S., Zhang J., Zhong A., Wu F., *Mater. Chem. Front.*, **2021**, *5*(1), 406
[66] Zhang Z., Xu W., Kang M., Wen H., Guo H., Zhang P., Xi L., Li K., Wang L., Wang D., Tang B. Z., *Adv. Mater.*, **2020**, *32*(36), e2003210
[67] Li Y., Wu Q., Kang M., Song N., Wang D., Tang B. Z., *Biomaterials*, **2020**, *232*, 119749
[68] Wan Q., Zhang R., Zhuang Z., Li Y., Huang Y., Wang Z., Zhang W., Hou J., Tang B. Z., *Adv. Funct. Mater.*, **2020**, *30*(39), 2002057
[69] Shi L., Wu W., Duan Y., Xu L., Xu Y., Hou L., Meng X., Zhu X., Liu B., *Angew. Chem. Int. Ed.*, **2020**, *59*(43), 19168
[70] Qi S., Kim S., Nguyen V. N., Kim Y., Niu G., Kim G., Kim S. J., Park S., Yoon J., *ACS Appl. Mater. Interfaces*, **2020**, *12*(46), 51293
[71] Yu Y., Zhang W., Gong Q. T., Liu Y. H., Yang Z. J., He W. X., Wang N., Yu X. Q., *J. Biotechnol.*, **2020**, *324*, 91
[72] Zhu D. M., Duo Y. H., Suo M., Zhao Y. H., Xia L. G., Zheng Z., Li Y., Tang B. Z., *Angew. Chem. Int. Ed.*, **2020**, *59*(33), 13836
[73] Huang J. C., He B. Z., Zhang Z. J., Li Y. M., Kang M. M., Wang Y. W., Li K., Wang D., Tang B. Z., *Adv. Mater.*, **2020**, *32*(37), 2003382
[74] Choi S. K., Rho J. G., Yoon S. E., Seok J. H., Kim H., Min J., Yoon W., Lee S., Yun H., Kwon O. P., Kim J. H., Kim W., Kim E., *Bioconjugate Chem.*, **2020**, *31*(11), 2522
[75] Li Y. Y., Liu S. J., Ni H. W., Zhang H. K., Zhang H. Q., Chuah C., Ma C., Wong K. S., Lam J. W. Y., Kwok R. T. K., Qian J., Lu X. F., Tang B. Z., *Angew. Chem. Int. Ed.*, **2020**, *59*(31), 12822
[76] OwYong T. C., Ding S. Y., Wu N., Fellowes T., Chen S. J., White J. M., Wong W. W. H., Hong Y. N., *Chem. Commun.*, **2020**, *56*, 14853
[77] Zhou T., Zhu J. F., Shang D., Chai C. X., Li Y. Z., Sun H. Y., Li Y. Q., Gao M., Li M., *Mater. Chem. Front.*, **2020**, *4*, 3201
[78] Liu J. J., Liu X. G., Wu M., Qi G. B., Liu B., *Nano Lett.*, **2020**, *20*(10), 7438
[79] Zhu C., Kwok R. T. K., Lam J. W. Y., Tang B. Z., *ACS Appl. Bio Mater.*, **2018**, *1*, 1768
[80] Zhou Y., Hua J., Zhang H.-P., Tang Y., *Chem. Res. Chinese Universities*, **2021**, *37*(1), 110
[81] Li X., Zha M., Li Y., Ni J. S., Min T., Kang T., Yang G., Tang H., Li K., Jiang X., *Angew. Chem. Int. Ed.*, **2020**, *59*(49), 21899
[82] Zhang Z., Fang X. F., Liu Z. H., Liu H. C., Chen D. D., He S. Q., Zheng J., Yang B., Qin W. P., Zhang X. J., Wu C. F., *Angew. Chem. Int. Ed.*, **2020**, *59*, 3691
[83] Ma C., Xie G., Tao Y., Zhu H., Zhang Y., Chi Z., Liu S., Xu J., *Dyes and Pigments*, **2021**, *184*, 108776
[84] Guan X., Wang L., Liu M., Wang K., Yang X., Ding Y., Tong J., Lei Z., Lai S., *Mater. Chem. Front.*, **2021**, *5*(1), 355
[85] Fan W., Yung B., Huang P., Chen X., *Chem. Rev.*, **2017**, *117*, 13566
[86] Xiao Y. F., Xiang C., Li S., Mao C., Chen H., Chen J. X., Tian S., Cui X., Wan Y., Huang Z., Li X., Zhang X. H., Guo W., Lee C. S., *Small*, **2020**, *16*(34), e2002672
[87] Zhu W., Kang M., Wu Q., Zhang Z., Wu Y., Li C., Li K., Wang L., Wang D., Tang B. Z., *Adv. Funct. Mater.*, **2020**, doi: 10.1002/adfm.202007026
[88] Brindle K., *Nat. Rev. Cancer*, **2008**, *8*, 94
[89] Zhu H., Li Q., Shi B., Ge F., Liu Y., Mao Z., Zhu H., Wang S., Yu G., Huang F., Stang P. J., *Angew. Chem. Int. Ed.*, **2020**, *59*, 20208
[90] Hu Y., Cao X., Guo Y., Zheng X., Li D., Chen S.-K., Chen G., You J., *Anal. Bio. Chem.*, **2020**, *412*, 7811
[91] Wang R., Gu X., Li Q., Gao J., Shi B., Xu G., Zhu T., Tian H., Zhao C., *J. Am. Chem. Soc.*, **2020**, *142*(35), 15084
[92] Zhang W., Wang H., Li F., Chen Y., Kwok R. T. K., Huang Y., Zhang J., Hou J., Tang B. Z., *Chem. Commun.*, **2020**, *56*(93), 14613
[93] Su P., Liang L., Wang T., Zhou P., Cao J., Liu W.-S., Tang Y., *Chem. Engin. J*, **2020**, doi: 10.1016/j.cej.2020.127408
[94] Fan C., Wang Y.-L., Zhao P.-J., Qu H.-Q., Su Y.-X., Li C., Zhu M.-Q., *Bioconj. Chem.*, **2020** *31*(10), 2303